Hindawi
Journal of Chemistry
Volume 2019, Article ID 3258342, 10 pages
https://doi.org/10.1155/2019/3258342

Research Article

A Comprehensive Study on Hydroxyl Multiwalled Carbon Nanotubes Used as Catalysts for VO_2^+/VO^{2+} Reaction in Vanadium Redox Flow Battery

Qiang Li,[1] Anyu Bai,[1] Zeqiang Qu,[1] Tianyu Zhang,[1] Jie Li,[1] Xiaochen Zhang,[1] Mingfu Yu,[1] Zhichao Xue,[2] and Hong Sun [1]

[1]*School of Mechanical Engineering, Shenyang Jianzhu University, Shenyang 110168, China*
[2]*School of Science, Shenyang Jianzhu University, Shenyang 110168, China*

Correspondence should be addressed to Hong Sun; sunhongwxh@sina.com

Received 15 June 2019; Accepted 23 October 2019; Published 30 November 2019

Guest Editor: Lei Zhang

A comprehensive study on the hydroxyl multiwalled carbon nanotubes (hydroxyl MWCNTs) as catalysts in a positive reaction was performed to improve the efficiency of the vanadium redox flow battery (VRFB). The physicochemical properties of the hydroxyl MWCNT-modified electrode were characterized by using a scanning electron microscope (SEM), conductivity measurement, Brunner–Emmet–Teller (BET) measurement, X-ray photoelectron spectroscopy (XPS) analysis, cyclic voltammetry (CV) tests, electrochemical impedance spectroscopy (EIS) analysis, and charge-discharge tests. The prepared composite electrode possesses a huge amount of oxygen-containing groups, high-specific surface area, high electrical conductivity, and high catalytic activity towards the VO_2^+/VO^{2+} reaction based on physicochemical characterization. The hydroxyl MWCNT-modified graphite felt (hydroxyl MWCNTs/GF) shows the best cell performance with the energy efficiency of 79.74% and remains in high stability after 50 cycles. The improved cell performance is probably ascribed to the increase in active sites, fast charge transfer, and mass transfer rate of the introduced hydroxyl MWCNTs.

1. Introduction

With the gradual depletion of fossil energy, people around the world pay more and more attention to the development and utilization of renewable energy resources. However, renewable energy power generation, such as wind power and solar energy, has obvious discontinuities, instability, and uncontrollability. Therefore, the development and the use of large-scale and high-efficiency energy storage technologies are the basis for future changes in the energy system [1–5]. As one of the promising approaches for energy storage, VRFB has drawn great attention since it possesses advanced characteristics such as flexible battery assembly design, long cycle life, large battery capacity, low self-discharge, and no cross contamination [6–12].

In VRFB, carbonaceous materials have been widely used as electrode materials for the catalysis of the electrode reaction. GF is the most popular electrode in VRFB [13–15]. However, GF shows poor kinetic reversibility and electrochemical activity toward electrode reactions. Hence, most investigations are focused on the modification of GF to improve its electrochemical performance. Various approaches including thermal treatment, acid oxidation, ammoniated treatment, and nanoparticles modification of GF have been reported to form more active sites for the improvement of cell performance [16–19].

Carbon nanotubes (CNTs) or functionalized CNTs have been proved to be an excellent catalyst in batteries due to its superior electrical conductivity, mechanical strength, and chemical stability. Furthermore, the surface of CNTs is inherently more active than other graphitic variants and has faster electron transfer rate. Some literatures have focused on the investigation of CNTs as catalysts for VRFB electrodes. The application of single-walled CNTs used as

catalysts in VRFB was firstly reported by Li et al. [20]. The kinetic properties of V^{2+}/V^{3+} and VO^{2+}/VO_2^+ redox couples are improved by employing the graphite/CNT composite as electrodes. Moreover, functionalized CNTs exhibit higher electronic conductivity and thermal/chemical stability. Hence, more interests have been focused on the functionalized CNTs due to their unique physicochemical properties. Various efforts have been paid on the modification of CNTs for VRFB applications, including KOH activation [21], acid treatment [22], nitrogen and sulfur doping [23, 24], and combination with nanosheets or nanoparticles [25–27]. Among various kinds of catalysts, hydroxyl MWCNTs exhibit remarkable electrochemical performance. Li et al. investigated the MWCNTs functionalized with hydroxyl groups for the VO^{2+}/VO_2^+ redox reaction [28]. Compared with the pristine MWCNTs, the hydroxyl MWCNTs used as positive-electrode reaction catalysts exhibit better storage efficiency. However, the catalytic mechanism of the hydroxyl modified MWCNTs for the VO^{2+}/VO_2^+ redox reaction still remains unclear. A comprehensive study on physiochemical characteristic variation of electrodes after the modification of hydroxyl MWCNTs should be further investigated to reveal the catalytic mechanism of hydroxyl MWCNTs.

In this paper, hydroxyl MWCNTs were used as electrode catalysts, while pristine MWCNTs were used as a comparison. The characteristics of the prepared hydroxyl MWCNTs/GF were tested by using SEM, four-point probes, BET method, and XPS. The electrochemical performance of the hydroxyl MWCNT-modified electrodes for VO^{2+}/VO_2^+ redox couple was analyzed by carrying out the tests of CV, EIS, and charge-discharge.

2. Experimental

2.1. Reagents and Materials. All chemical reagents which were of analytical reagent grade were directly used without purification. Deionized water was used to wash the modified GF and prepare the electrolyte. Sulfuric acid with the concentration of 98 wt% was used as the supporting electrolyte. Nafion 117 membrane, GF with a thickness of 5 mm, and graphite plates were used for the assembling of the cell unit. The MWCNTs and hydroxyl MWCNTs were purchased from Beijing DK nanotechnology Co. Ltd.

2.2. Preparation

2.2.1. Immobilization of MWCNTs and Hydroxyl MWCNTs on GCE. A glassy carbon electrode (GCE, diameter 3 mm) was firstly polished with aqueous slurries of alumina powders on a polishing microcloth. Then, the electrode was rinsed by deionized water and ultrasonic processed in ethanol for 3 times. The suspension containing catalysts was prepared by ultrasonically mixing 10 mL dimethyl formamide with 10 mg MWCNTs and 10 mg hydroxyl MWCNTs, respectively. The decorated GCE was achieved by dropping 20 μL prepared suspension onto the surface of GCE, followed by evaporation in an oven at 45°C for 8 h. The GCE without modification was used as a comparison.

2.2.2. Preparation of MWCNTs/GF and Hydroxyl MWCNTs/GF. Prior to the modification of the GF electrode, a GF (3 cm × 3 cm) was washed by ultrasonication for 30 min in deionized water and then dried in an oven at 100°C for 4 h. The purified GF was immersed in the prepared suspension as mentioned in Section 2.2.1. Then, the modified GF was purified by deionized water and dried in an oven at 100°C for 24 h. The composite electrode with the modification of hydroxyl MWCNTs was also prepared as stated above.

2.3. Characterization of Modified Electrode

2.3.1. Material Characterization. The surface morphology and the specific surface area of the prepared electrode were measured by SEM (Hitachi, S4800) and BET method (Micromeritics TriStar II 3020), respectively. The conductivity of the prepared electrode was measured by four-point probes (RTS-8, Four Probes Tech). The nitrogen doping level and doping type in the modified composite electrode were evaluated by XPS (Thermo Fisher Scientific, EscaLab 250 XI system).

2.3.2. Electrochemical Tests. The CV results were obtained by PARSTAT 4000+ workstation over the voltage range from −0.2 V to 1.6 V. The EIS tests were operated by applying an alternating voltage of 5 mV over the frequency range of 0.01 Hz to 100 kHz. A three-electrode cell was employed to characterize the electrochemical performance of hydroxyl MWCNT-modified electrode. The three-electrode cell was equipped with the hydroxyl MWCNT-modified glassy carbon electrode (hydroxyl MWCNTs/GCE) as a working electrode, a Pt electrode as a counter electrode, and a saturated calomel electrode as a reference electrode. The electrolyte used in the cell was 0.1 M $VOSO_4$ + 2 M H_2SO_4 aqueous solution.

Charge-discharge tests were conducted by using an assembly home-made static battery test system. The prepared hydroxyl MWCNT-modified electrode was used as a positive electrode in charge-discharge tests. The anolyte for VRFB was 1 M V^{3+} + 4.2 M H_2SO_4, and the catholyte was 1 M VO^{2+} + 4.2 M H_2SO_4. The upper and lower voltage limits for the charge-discharge test were 1.65 V and 0.8 V, respectively. The durability of the prepared hydroxyl MWCNTs/GF electrode was evaluated by 50 cycles of charge-discharge tests.

3. Results and Discussion

3.1. Material Property Characterization

3.1.1. SEM Tests. The morphology of pristine GF and hydroxyl MWCNTs/GF was characterized by using SEM. As shown in Figure 1, the surface of pristine GF is smooth. After treatment, the surface of GF is covered by attachments, indicating that the hydroxyl MWCNTs have been successfully attached to GF.

3.1.2. Conductivity Measurement. The conductivities of pristine GF, MWCNTs/GF, and hydroxyl MWCNTs/GF

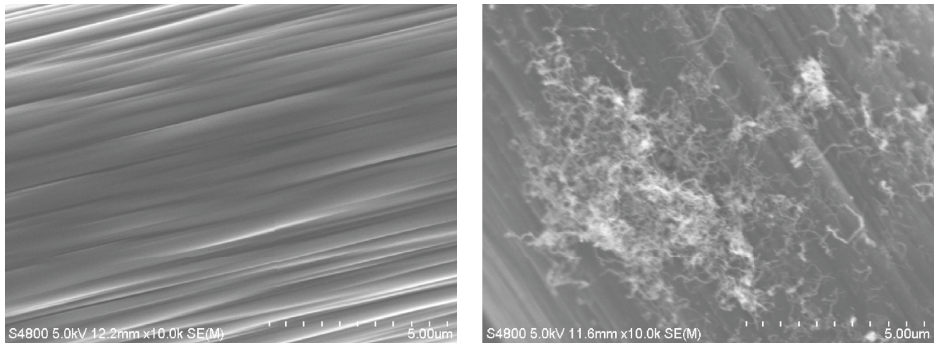

(a) (b)

Figure 1: SEM images of pristine GF and (a) hydroxyl MWCNTs/GF (b).

were measured by four-point probes (RTS-8, Four Probes Tech). The results are listed in Table 1. It is obvious that the conductivity of GF is significantly increased due to the modification of MWCNTs. Compared to MWCNTs/GF, the conductivity of hydroxyl MWCNTs/GF has a slightly lower value of 54.58 S/cm, suggesting that the modification of hydroxyl MWCNTs does not lead to an obvious decrease in conductivity. The increase in the conductivity of electrode is owing to the modification of hydroxyl MWCNTs which is a benefit for electron transfer during the electrochemical reaction, resulting in a decrease in ohmic polarization.

3.1.3. Specific Surface Area Test. The specific surface area of electrode has a significant influence on cell performance since electrode with high specific area attracts more vanadium ions and provides more active sites for the electrochemical reaction. The influence of hydroxyl MWCNTs modification on the specific surface area of GF was evaluated by the BET method. The nitrogen adsorption-desorption isotherms of GF, MWCNTs/GF, and hydroxyl MWCNTs/GF are presented in Figure 2. It is clear that there is a typical IV isotherm for all samples, indicating the presence of the porous structure. The measured specific surface areas of GF, MWCNTs/GF, and hydroxyl MWCNTs/GF were 0.86 m^2/g, 6.19 m^2/g, and 11.10 m^2/g, respectively. The results indicate that the specific surface area of the prepared electrode is significantly increased due to the decoration of hydroxyl MWCNTs. The specific area of hydroxyl MWCNTs/GF is higher than that of MWCNTs/GF. The reason may due to the fact that the hydroxyl groups in hydroxyl MWCNTs are a benefit for the adsorption of hydroxyl MWCNTs on the GF surface, resulting in a large number of hydroxyl MWCNTs adsorbed on the GF surface during the immersion process.

(1) XPS Test. In order to compare the main element contents on the surface of pristine GF, MWCNTs/GF, and hydroxyl MWCNTs/GF, XPS tests were performed in the binding energy range of 0–1350 eV. Figure 3 is the scanning spectra of pristine GF, MWCNTs/GF, and hydroxyl MWCNTs/GF. There are two peaks located at 284 eV and 532 eV, corresponding to C and O elements, respectively. The content of C, O, and N elements calculated from XPS scan data is listed

Table 1: Resistivity and conductivity of different samples.

Measured samples	Conductivity (S/cm)
Pristine GF	47.62
MWCNTs/GF	62.50
Hydroxyl MWCNTs/GF	66.67

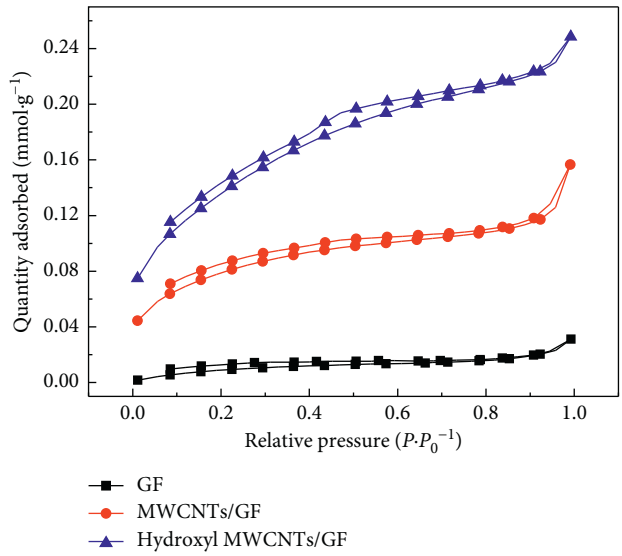

Figure 2: Nitrogen adsorption-desorption isotherms.

in Table 2. As shown in Table 2, the content of O element increases from 2.17% to 13.02% after the decoration of hydroxyl MWCNTs, suggesting that the oxygen-containing groups have been successfully decorated onto the GF surface. Figure 3(f) is the C1s plot of the hydroxyl MWCNTs/GF that can be fitted by convolving into four peaks, namely, C=C (284.5 eV), C-C (286.2 eV), C-O (287.5 eV), and C=O (287.9 eV). Comparing Figure 3(f) with Figure 3(d), it can be seen that the content of the C-O bond in the hydroxyl MWCNTs/GF is significantly improved. The content of the C-O bond in the hydroxyl MWCNTs/GF is 16.2%, which is much higher than that in MWCNTs/GF (4.60%) and pristine GF (3.64%). The results indicate that the hydroxyl MWCNTs/GF has more oxygen-containing groups,

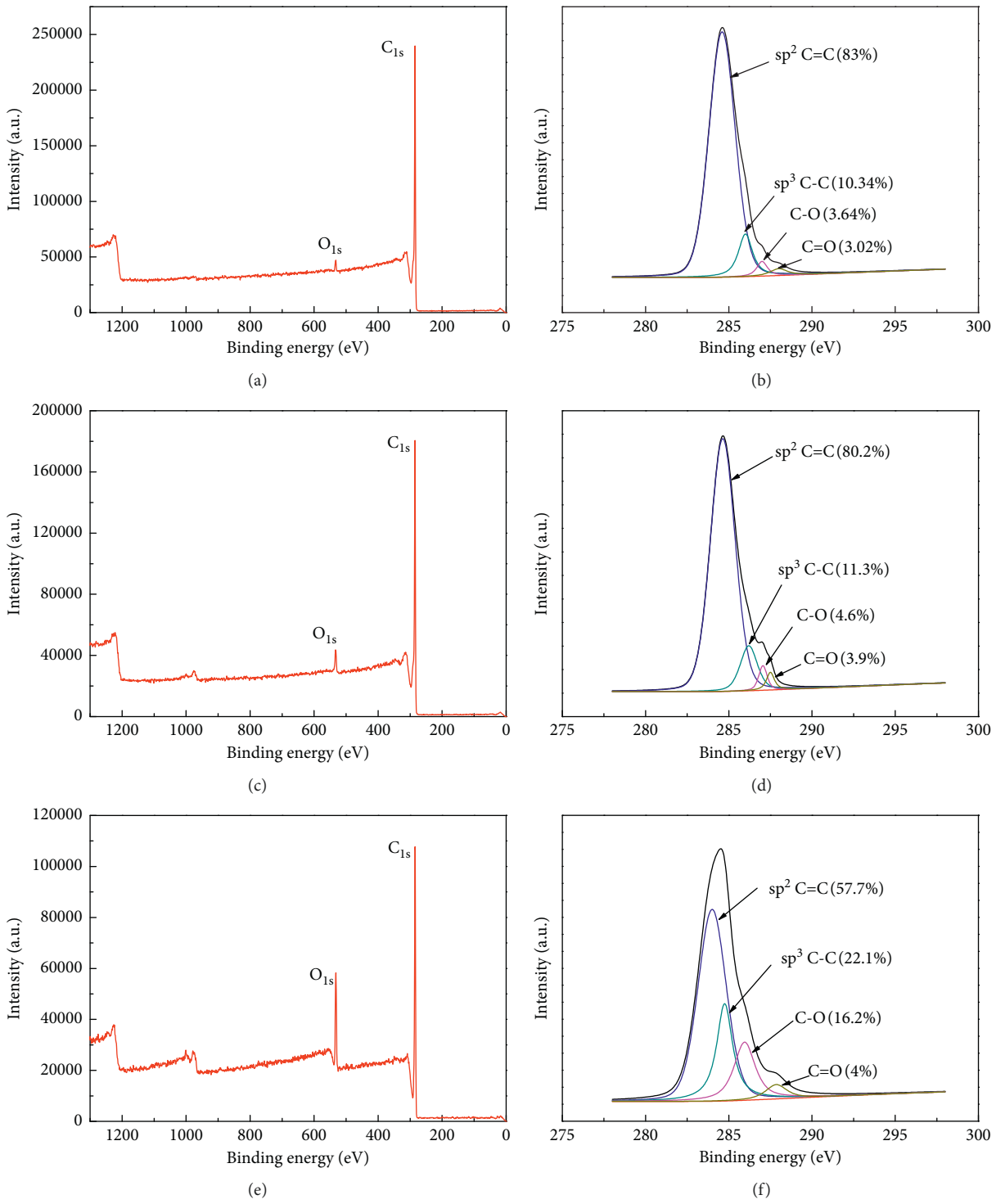

Figure 3: XPS spectra and curve fit of C1s spectra from pristine GF (a, b), MWCNTs/GF (c, d), and hydroxyl MWCNTs/GF (e, f).

especially the C-O bond containing groups, which show high catalytic activity toward the VO_2^+/VO^{2+} reaction.

3.2. Electrochemical Performance

3.2.1. Cyclic Voltammetry Test. Cyclic voltammetry tests were carried out in 0.1 M $VOSO_4$ + 2 M H_2SO_4 electrolyte from −0.2 V to 1.6 V. The CV curves of GCE, MWCNTs/GCE, and hydroxyl MWCNTs/GCE at different scan rates are shown in Figures 4(a)–4(c). It is obvious that only the oxidation peak of the VO_2^+/VO^{2+} redox reaction is observed when the pristine GCE is used as a working electrode, indicating that an irreversible VO_2^+/VO^{2+} redox reaction is taken place on the pristine GCE. After the modification of MWCNTs, the electrode has symmetric oxidation and

Table 2: Content of C, O, and N elements in hydroxyl MWCNTs/GF, MWCNTs/GF, and pristine GF.

Tested samples	Carbon content (%)	Oxygen content (%)	Nitrogen content (%)
Pristine GF	97.31	2.17	0.52
MWCNTs/GF	95.83	3.56	0.61
Hydroxyl MWCNTs/GF	86.25	13.02	0.74

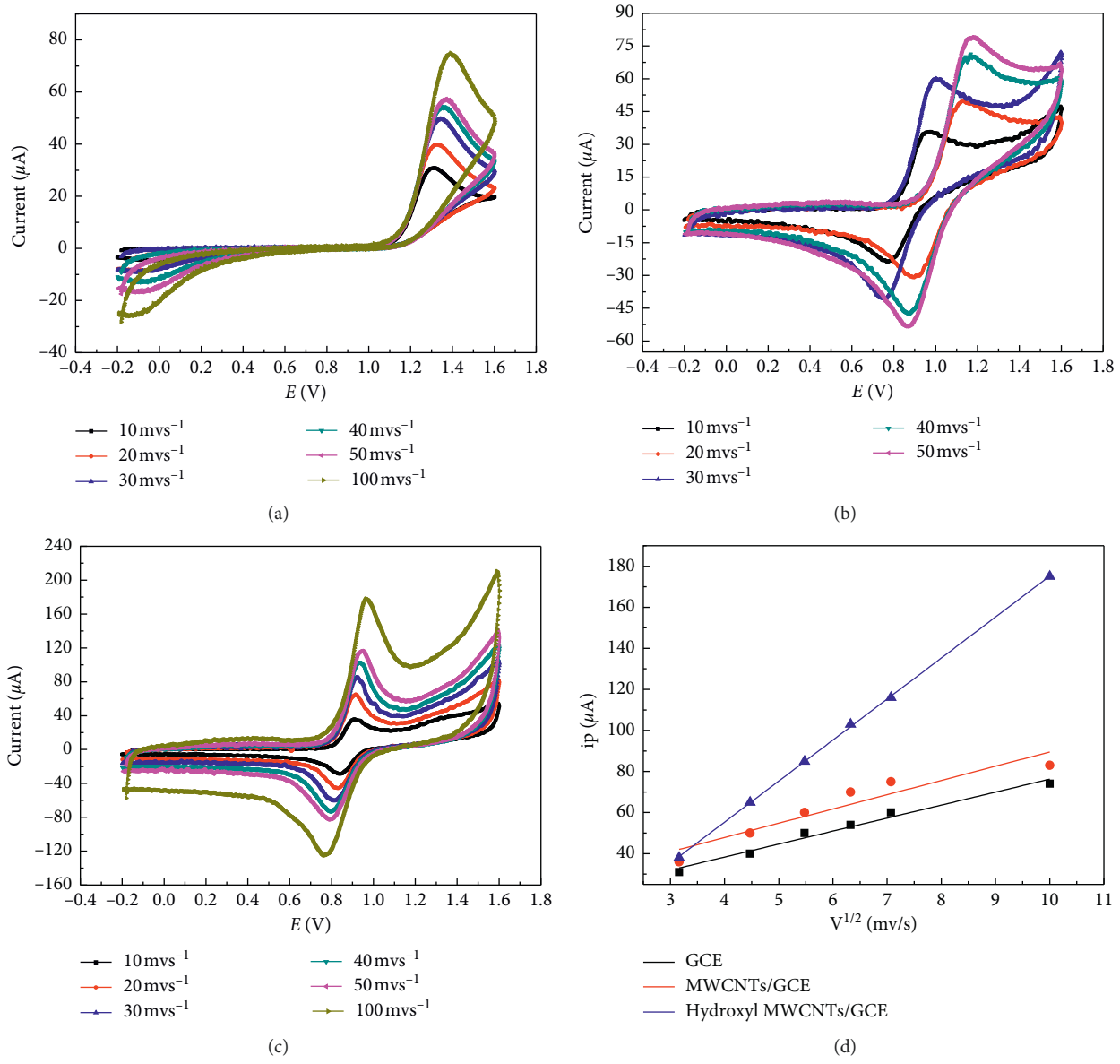

Figure 4: Cyclic voltammetry curves of GCE (a), MWCNTs/GCE (b), and hydroxyl MWCNTs/GCE (c) under different scan rates in 0.1 M $VOSO_4$ + 2 M H_2SO_4 and the relationship between oxidation peak currents and square root of scan rate (d).

reduction peaks. Furthermore, the reduction peak becomes obvious and the oxidation peak increases, as shown in Figure 4(b). For hydroxyl MWCNTs/GCE, the peak potential separation is almost unchanged with increasing scan rate, meaning that the VO_2^+/VO^{2+} redox reaction on the hydroxyl MWCNTs/GCE surface is a quasireversible reaction. Moreover, it can be seen that the redox peak currents of hydroxyl MWCNTs/GCE are the highest among these samples, while the potential separation is the lowest, indicating that the electrode modified with hydroxyl MWCNTs has the best performance.

Since the mass transfer plays an important role on cell performance, the mass transfer properties of active species in the modified electrodes were evaluated by plotting the

oxidation peak currents versus the square root of scan rate, as shown in Figure 4(d). The peak currents are approximately proportional to the square root of scan rate for all tested samples, indicating that the reactions in all electrodes are mass transfer controlled. In Figure 4(d), the slope of the fitted line positively represents the mass transfer velocity of active species. It should be noted that the slope for the hydroxyl MWCNTs/GCE is the largest, indicating that the hydroxyl MWCNTs potentially facilitate the diffusion of active species, which is a benefit for the decrease in concentration polarization. The reason may be due to the introduction of hydroxyl MWCNTs which show large numbers of oxygen-containing groups, resulting in a high hydrophilicity and high catalytic activity of the modified electrode.

The CV tests of different electrodes at a scan rate of 20 mV/s are shown in Figure 5. By comparing the voltammetric behavior of different electrodes, the results show that the electrochemical activity of GCE is significantly enhanced after the modification of hydroxyl MWCNTs.

The peak currents and peak potential separation (ΔE_p) values are listed in Table 3. The electrode modified with hydroxyl MWCNTs show the best catalytic activity with the oxidation peak current I_{pa} of 64.34 μA and the reduction peak current I_{pc} of −53.61 μA, respectively. In comparison to the MWCNTs/GCE, the hydroxyl MWCNTs/GCE has abundant hydroxyl groups, indicating that the hydroxyl MWCNTs are electrochemically more accessible for electrode reactions, resulting in an improvement in VRFB performance. Furthermore, ΔE_p decreases after the modification with hydroxyl MWCNTs, meaning that the modification of hydroxyl MWCNTs is also a benefit for the improvement of electrochemical reversibility. Compared with MWCNTs/GCE, hydroxyl MWCNTs/GCE delivers better electrochemical reversibility toward the positive redox couple. The results indicate that plenty of hydroxyl groups attached on hydroxyl MWCNTs can efficiently facilitate the positive-reaction rate and decrease the electrochemical polarization for the VO^{2+}/VO_2^+ reaction.

3.2.2. EIS Test. The electrochemical impedance spectroscopy tests were carried out to further investigate the effect of hydroxyl MWCNTs on the positive VO^{2+}/VO_2^+ reaction. The corresponding Nyquist plot is shown in Figure 6. For cells with hydroxyl MWCNT-decorated electrode, the Nyquist plot is composed of a semicircle and a linear part in the frequency range from 0.01 Hz to 100 kHz. The semicircle part at high frequency represents the charge transfer process, and the linear part at low frequency reflects the mass diffusion process during the electrochemical reaction. The results demonstrate that the VO^{2+}/VO_2^+ couple reaction is both controlled by charge transfer and mass transfer. The spectra can be fitted by an equivalent circuit. In the equivalent circuit, R_1 is the ohmic resistance and R_2 represents the charge transfer resistance across the electrode/electrolyte interface. Q is the constant phase element, reflecting the electric double-layer capacitance of the electrode/electrolyte interface. W is the Warburg impedance,

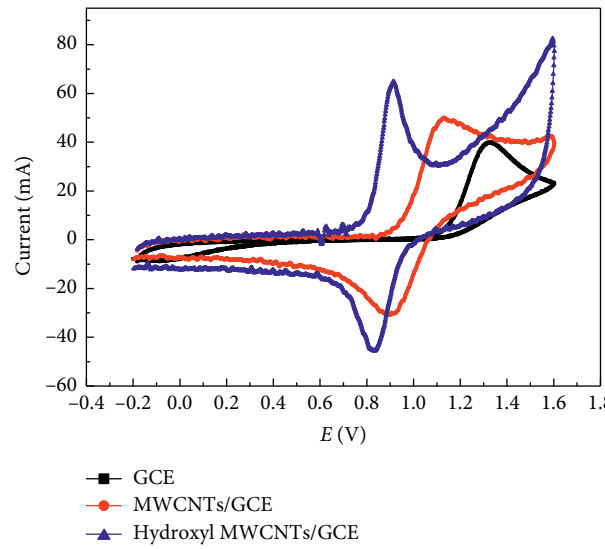

Figure 5: CV curves of different electrodes at a constant scan rate of 20 mV/s.

which is relevant to vanadium ion adsorption and diffusion in electrodes.

The parameters obtained from the equivalent circuit are listed in Table 4. A significant decrease in R_2 is observed, indicating that the charge transfer resistance at the electrode/electrolyte interface decreases after the decoration of MWCNTs and hydroxyl MWCNTs. The hydroxyl MWCNTs/GF shows the lowest charge transfer resistance because the oxygen-containing groups on hydroxyl MWCNTs decrease the electrochemical polarization and facilitate the charge transfer across the solution/electrode interface, thus confirming the beneficial role of hydroxyl MWCNTs. According to Table 4, the value of Q increases after the treatment of GF. The increase in the Q value indicates that the modified electrodes are more adsorptive for vanadium ions, resulting in a decrease in mass transfer resistance. The hydroxyl MWCNTs/GF shows the largest Q value because the relatively high negative charge density of oxygen-containing groups in hydroxyl MWCNTs potentially accelerate the adsorption for vanadium ions by electrostatic force and facilitate the mass transfer of active species [29, 30]. The Warburg coefficient for different samples is depicted in Table 4. The hydroxyl MWCNTs/GF shows the largest value of the Warburg coefficient, implying that the active species diffusion is fast in hydroxyl MWCNTs/GF. Both EIS and CV results show that reaction kinetics of VO^{2+}/VO_2^+ on the surface of the hydroxyl MWCNTs/GF electrode is faster than that of other electrodes.

3.2.3. Charge-Discharge Test. For a further understanding on the influence of MWCNTs on the performance of VRFB, the charge-discharge tests were conducted by cells equipped with different electrodes, as shown in Figure 7. All cells were charged to the upper voltage of 1.65 V and discharged to the lower voltage of 0.8 V at a constant current density of 80 mA/cm^2. The thickness of GF was 5 mm, and the flow velocity of

Table 3: Parameters obtained from CV tests with different catalysts at a scan rate of 20 mV/s.

Samples	Peak potential separation (ΔE_p (mV))	Reduction peak current (I_{pc} (μA))	Oxidation peak current (I_{pa} (μA))
GCE	1100.13	−15.31	30.45
MWCNTs/GCE	153.43	−38.22	45.53
Hydroxyl MWCNTs/GCE	81.52	−53.61	64.34

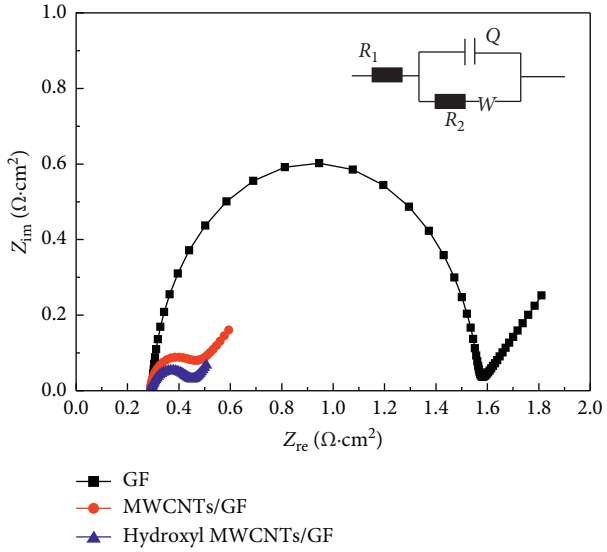

Figure 6: EIS spectra of cells with different electrodes and fitted equivalent circuit.

Table 4: Fitted parameters resulting from the equivalent circuit model.

Different electrodes	R_1 (Ω·cm^2)	Q (CPE)		R_2 (Ω·cm^2)	W (S·s^5·cm^2)
		Q/Y·(S·s^{-n})$^{-1}$	N ($0 < n < 1$)		
Pristine GF	0.40	1.19×10^{-3}	0.74	1.26	0.11
MWCNTs/GF	0.27	2.34×10^{-3}	0.86	0.16	0.32
Hydroxyl MWCNTs/GF	0.23	4.53×10^{-3}	0.94	0.14	0.44

electrolyte was 30 ml/min. As observed, the charge-discharge curves reveal that the cell employing hydroxyl MWCNTs as catalysts shows the best cell performance, resulting in a lowest charge voltage and a largest discharge voltage. Compared to the cell equipped with the pristine electrode, the battery capacities of cells equipped with MWCNTs and hydroxyl MWCNT-modified electrodes increase by 18.71% and 27.60%, respectively. The significant increase in capacity is attributed to the high specific surface, the high conductivity, and high catalytic activity of hydroxyl MWCNTs/GF electrode, leading to a better cell performance.

The current efficiency (CE), voltage efficiency (VE), and energy efficiency (EE) of cells with different electrodes are shown in Table 5. The cell with hydroxyl MWCNT-modified electrode exhibits substantially improved VE of 83.05% and EE of 79.74%, respectively. The difference in EE reflects the difference in the catalytic activity and mass transfer property of electrode materials. The improved performance for hydroxyl MWCNTs/GF may be ascribed to the high conductivity and high specific surface area of the modified hydroxyl MWCNTs. Furthermore, the introduction of oxygen-containing groups in hydroxyl MWCNTs significantly decrease the charge transfer resistance between electrolyte/electrode interface while increase the mass diffusion rate of vanadium ions during the electrochemical reaction.

3.2.4. Cyclic Stability Test. Cyclic stability tests were carried out at a constant current density of 80 mA/cm^2 to evaluate the durability of hydroxyl MWCNT catalysts. The cycling performance including CE, EE, and discharge retention is shown in Figure 8. It is obvious that the CE of two cells remains nearly stable during the whole cyclic stability test. The CEs for two cells are higher than 95%, demonstrating good airtightness of the battery setup. As for EE, the VRFB with hydroxyl MWCNTs/GF shows much higher EE than the GF-based VRFB. The EE of VRFB with GF decreases from 74.61% to 71.45%, while the EE of VRFB with hydroxyl MWCNTs/GF remains nearly stable with the value of 79.88%. Consequently, the initial discharge capacity of VRFB with hydroxyl MWCNTs/GF is higher than that of

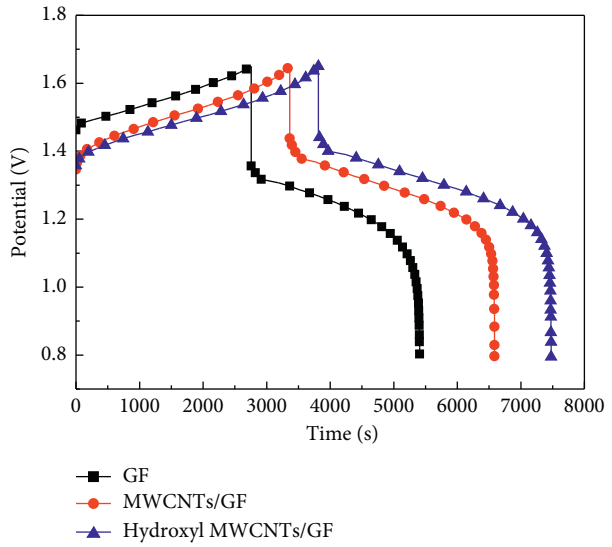

Figure 7: Charge-discharge curves of different electrodes.

Table 5: Efficiency of cells equipped with different electrodes.

Different electrodes	Current efficiency (CE) (%)	Voltage efficiency (VE) (%)	Energy efficiency (EE) (%)
Pristine GF	96.21	75.87	72.99
MWCNTs/GF	95.92	81.32	78.01
Hydroxyl MWCNTs/GF	96.01	83.05	79.74

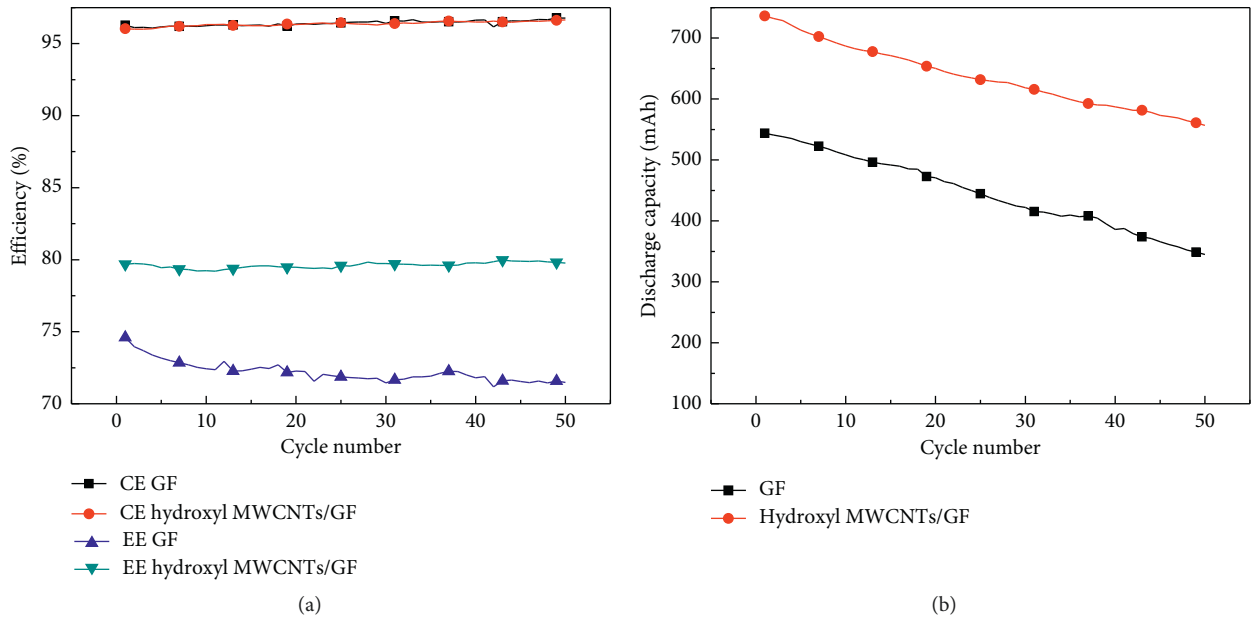

Figure 8: Variation of cell efficiency (a) and discharge capacity (b) after 50 cycles of charge-discharge tests for cells equipped with GF and hydroxyl MWCNTs/GF electrode.

GF-based VRFB, as shown in Figure 8(b). The discharge capacity of VRFB with hydroxyl MWCNTs/GF is 736.20 mAh at the 1th cycle compared to 543.70 mAh of GF-based VRFB, while the values decrease to 556.8 mAh and 344.80 mAh at the 50th cycle, respectively. The stable EE and the slow capacity decay demonstrate the excellent cycling stability of hydroxyl MWCNT catalysts under VRFB operation conditions, which is ascribed to the enhanced

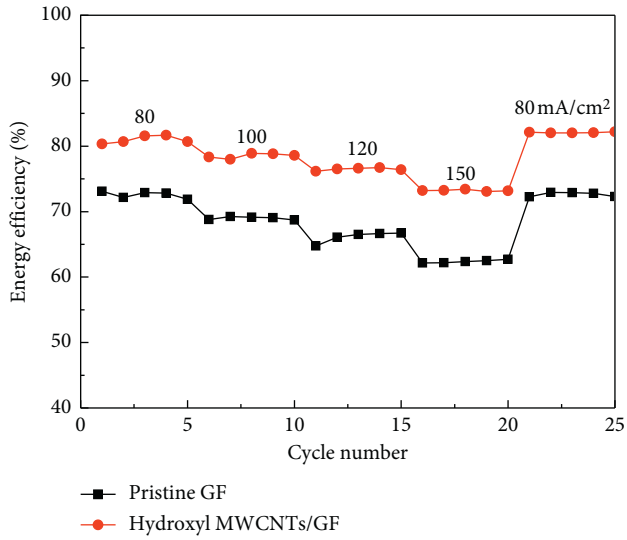

Figure 9: Variation of the EE of pristine GF and hydroxyl MWCNTs/GF-based single cells operating at the current density range of 80 mA/cm^2 to 150 mA/cm^2.

electrochemical catalytic activity and reversibility of the hydroxyl MWCNTs/GF electrode.

Figure 9 shows the energy efficiency variation of pristine GF and hydroxyl MWCNTs/GF-based single cells operated at different current densities. The current density was ranged from 80 mA/cm^2 to 150 mA/cm^2. It can be noted that the energy efficiencies of pristine GF and hydroxyl MWCNTs/GF-based cells are decreased with the current density increasing due to the increase in overvoltage. The energy efficiency of hydroxyl MWCNTs/GF-based cell decreases from 81.67% to 73.42% with the current density ranging from 80 mA/cm^2 to 150 mA/cm^2. Compared with the cell with pristine GF, the cell equipped with hydroxyl MWCNTs/GF shows higher efficiencies at different current densities. The higher energy efficiency of the hydroxyl MWCNTs/GF-based cell is attributed to the enhanced conductivity and increased reactive sites of hydroxyl MWCNTs/GF electrode, resulting in improved overall cell performance [31, 32].

4. Conclusions

Based on the experimental results, VRFB assembled with hydroxyl MWCNTs/GF show significantly improved electrochemical performance. The results support that the hydroxyl MWCNTs modified on GF reduce the electrochemical polarization of the cell, decrease the ohmic and mass transfer resistance, and improve the electrochemical reversibility. The enhanced performance for hydroxyl MWCNTs/GF-based battery is not only related to the introduction of oxygen-containing groups on the hydroxyl MWCNTs surface but also due to the high conductivity and high specific surface area of the hydroxyl MWCNTs. The investigation demonstrates that the newly developed hydroxyl MWCNT-modified GF holds great promise in the application of VRFB.

Data Availability

The data used to support the findings of this study are available from the corresponding author upon request.

Conflicts of Interest

The authors declare that there are no conflicts of interest regarding the publication of this paper.

Acknowledgments

This research was supported by the National Natural Science Foundation of China (51902211, 51476107, and 51776131), Liaoning Revitalization Talents Program (XLYC1802045), and the Foundation from Liaoning Province of China (20170540746 and LJZ2016013).

References

[1] S. L. Huang, H. F. Yu, and Y. S. Lin, "Modification of Nafion® membrane via a sol-gel route for vanadium redox flow energy storage battery applications," *Journal of Chemistry*, vol. 2017, Article ID 4590952, 10 pages, 2017.

[2] N. Xu, X. Li, X. Zhao, J. B. Goodenough, and K. Huang, "A novel solid oxide redox flow battery for grid energy storage," *Energy & Environmental Science*, vol. 4, no. 12, pp. 4942–4946, 2011.

[3] Z. Yang, J. Liu, S. Baskaran, C. H. Imhoff, and J. D. Holladay, "Enabling renewable energy—and the future grid—with advanced electricity storage," *JOM*, vol. 62, no. 9, pp. 14–23, 2010.

[4] M. Skyllas-Kazacos, "10-electro-chemical energy storage technologies for wind energy systems," in *Stand-Alone and Hybrid Wind Energy Systems*, pp. 323–365, Woodhead Publishing, Cambridge, UK, 2010.

[5] G. Kear, A. A. Shah, and F. C. Walsh, "Development of the all-vanadium redox flow battery for energy storage: a review of technological, financial and policy aspects," *International Journal of Energy Research*, vol. 36, no. 11, pp. 1105–1120, 2012.

[6] M. Skyllas-Kazacos, M. Robins, R. G. Fane, and A. G. Green, "New all-vanadium redox flow cell," *Journal of the Electrochemical Society*, vol. 133, no. 5, pp. 1057-1058, 1986.

[7] M. Park, J. Ryu, W. Wang, and J. Cho, "Material design and engineering of next-generation flow-battery technologies," *Nature Reviews Materials*, vol. 2, no. 1, p. 16080, 2017.

[8] B. P. Hayes, A. Wilson, R. Webster, and S. Z. Djokic, "Comparison of two energy storage options for optimum balancing of wind farm power outputs," *IET Generation, Transmission & Distribution*, vol. 10, no. 3, pp. 832–839, 2016.

[9] M. Skyllas-Kazacos, M. H. Chakrabarti, S. A. Hajimolana, F. S. Mjalli, and M. Saleem, "Progress in flow battery research and development," *Journal of the Electrochemical Society*, vol. 158, no. 8, pp. R55–R79, 2011.

[10] L. Yue, W. Li, F. Sun, L. Zhao, and L. Xing, "Highly hydroxylated carbon fibres as electrode materials of all-vanadium redox flow battery," *Carbon*, vol. 48, no. 11, pp. 3079–3090, 2010.

[11] Y. Lv, L. Zhang, G. Cheng et al., "Preparation of carbon nanosheet by molten salt route and its application in

catalyzing VO^{2+}/VO_2^+ redox reaction," *Journal of The Electrochemical Society*, vol. 166, no. 6, pp. A953–A959, 2019.

[12] Y. Jiang, X. Feng, G. Cheng et al., "Electrocatalytic activity of MnO_2 nanosheet array-decorated carbon paper as superior negative electrode for vanadium redox flow batteries," *Electrochimica Acta*, vol. 322, Article ID 134754, 2019.

[13] Q. Li, J. Q. Liu, A. Y. Bai et al., "Preparation of a nitrogen-doped reduced graphene oxide-modified graphite felt electrode for VO^{2+}/VO_2^+ reaction by freeze-drying and pyrolysis method," *Journal of Chemistry*, vol. 2019, Article ID 8958946, 9 pages, 2019.

[14] M. Etienne, J. F. Vivo-Vilches, I. Vakulko et al., "Layer-by-layer modification of graphite felt with MWCNT for vanadium redox flow battery," *Electrochimica Acta*, vol. 313, pp. 131–140, 2019.

[15] H. R. Jiang, W. Shyy, L. Zeng, R. H. Zhang, and T. S. Zhao, "Highly efficient and ultra-stable boron-doped graphite felt electrodes for vanadium redox flow batteries," *Journal Of Materials Chemistry A*, vol. 6, no. 27, pp. 13244–13253, 2018.

[16] B. Sun and M. Skyllas-Kazacos, "Chemical modification of graphite electrode materials for vanadium redox flow battery application-part II. Acid treatments," *Electrochimica Acta*, vol. 37, no. 13, pp. 2459–2465, 1992.

[17] S. Abbas, H. Lee, J. Hwang et al., "A novel approach for forming carbon nanorods on the surface of carbon felt electrode by catalytic etching for high-performance vanadium redox flow battery," *Carbon*, vol. 128, pp. 31–37, 2018.

[18] W. Wang, X. Wang, M. Guo, and J. Li, "Different treatments for positive and negative electrode materials of an all-vanadium redox flow battery," *Journal of University Science and Technology Beijing*, vol. 29, no. 1001, pp. 1141–1144, 2006.

[19] A. W. Bayeh, D. M. Kabtamu, Y.-C. Chang et al., "Ta_2O_5-nanoparticle-modified graphite felt as a high-performance electrode for a vanadium redox flow battery," *ACS Sustainable Chemistry & Engineering*, vol. 6, no. 3, pp. 3019–3028, 2018.

[20] W. Li, J. Liu, and C. Yan, "The electrochemical catalytic activity of single-walled carbon nanotubes towards VO_2^+/VO^{2+} and V^{3+}/V^{2+} redox pairs for an all vanadium redox flow battery," *Electrochimica Acta*, vol. 79, pp. 102–108, 2012.

[21] L. Dai, Y. Jiang, W. Meng, H. Zhou, L. Wang, and Z. He, "Improving the electrocatalytic performance of carbon nanotubes for VO^{2+}/VO_2^+ redox reaction by KOH activation," *Applied Surface Science*, vol. 401, pp. 106–113, 2017.

[22] W. Li, J. Liu, and C. Yan, "Modified multiwalled carbon nanotubes as an electrode reaction catalyst for an all vanadium redox flow battery," *Journal of Solid State Electrochemistry*, vol. 17, no. 5, pp. 1369–1376, 2013.

[23] S. Wang, X. Zhao, T. Cochell, and A. Manthiram, "Nitrogen-doped carbon nanotube/graphite felts as advanced electrode materials for vanadium redox flow batteries," *The Journal of Physical Chemistry Letters*, vol. 3, no. 16, pp. 2164–2167, 2012.

[24] C. Li, B. Xie, J. Chen, J. He, and Z. He, "Enhancement of nitrogen and sulfur co-doping on the electrocatalytic properties of carbon nanotubes for VO^{2+}/VO_2^+ redox reaction," *RSC Advances*, vol. 7, no. 22, pp. 13184–13190, 2017.

[25] M. Park, Y.-j. Jung, J. Kim, H. I. Lee, and J. Cho, "Synergistic effect of carbon nanofiber/nanotube composite catalyst on carbon felt electrode for high-performance all-vanadium redox flow battery," *Nano Letters*, vol. 13, no. 10, pp. 4833–4839, 2013.

[26] P. Han, Y. Yue, Z. Liu et al., "Graphene oxide nanosheets/multi-walled carbon nanotubes hybrid as an excellent electrocatalytic material towards VO^{2+}/VO_2^+ redox couples for vanadium redox flow batteries," *Energy & Environmental Science*, vol. 4, no. 11, pp. 4710–4717, 2011.

[27] G. Wei, X. Fan, J. Liu, and C. Yan, "Electrospun carbon nanofibers/electrocatalyst hybrids as asymmetric electrodes for vanadium redox flow battery," *Journal of Power Sources*, vol. 281, pp. 1–6, 2015.

[28] W. Li, J. Liu, and C. Yan, "Multi-walled carbon nanotubes used as an electrode reaction catalyst for VO_2^+/VO^{2+} for a vanadium redox flow battery," *Carbon*, vol. 49, no. 11, pp. 3463–3470, 2011.

[29] L. Wu, Y. Shen, L. Yu, J. Xi, and X. Qiu, "Boosting vanadium flow battery performance by nitrogen-doped carbon nanospheres electrocatalyst," *Nano Energy*, vol. 28, pp. 19–28, 2016.

[30] R. Wang and Y. Li, "Twin-cocoon-derived self-standing nitrogen-oxygen-rich monolithic carbon material as the cost-effective electrode for redox flow batteries," *Journal of Power Sources*, vol. 421, pp. 139–146, 2019.

[31] D.-S. Yang, J. Y. Lee, S.-W. Jo, S. J. Yoon, T.-H. Kim, and Y. T. Hong, "Electrocatalytic activity of nitrogen-doped CNT graphite felt hybrid for all-vanadium redox flow batteries," *International Journal of Hydrogen Energy*, vol. 43, no. 3, pp. 1516–1522, 2018.

[32] Y. C. Chang, Y. C. Shih, J. Y. Chen et al., "High efficiency of bamboo-like carbon nanotube on functionalized graphite felt as electrode in vanadium redox flow battery," *RSC Advances*, vol. 6, no. 104, Article ID 107294, 2016.